Electro-Fenton process at mild pH using Fe(III)-EDDS as soluble catalyst and carbon felt as cathode

Zhihong Ye, Enric Brillas, Francesc Centellas, Pere Lluís Cabot, Ignasi Sirés*

Laboratori d'Electroquímica dels Materials i del Medi Ambient, Departament de Química Física, Facultat de Química, Universitat de Barcelona, Martí i Franquès 1-11, 08028 Barcelona, Spain

Paper submitted to be published in *Applied Catalysis B: Environmental*

*Corresponding author: Tel.: +34 934039240; fax: +34 934021231.

E-mail address: i.sires@ub.edu (I. Sirés)

Abstract

The feasibility of destruction of organic pollutants in water at near-neutral pH by homogeneous electro-Fenton (EF) process employing a soluble Fe(III)–EDDS complex as catalyst is demonstrated for the first time. The performance of the Fe(III)–EDDS-assisted EF process with carbon-felt or air-diffusion cathodes was evaluated from the degradation of butylated hydroxyanisole (BHA) in sulfate medium. The influence of applied current, pH and Fe(III):EDDS ratio and dosage on BHA decay and mineralization was related to the evolution of H_2O_2 and iron concentrations. Using Fe(III)–EDDS, up to 50% Fe(II) regeneration was achieved in 10 min, whereas only 23% was transformed using hydrated Fe^{3+}. Almost total removal of BHA was achieved thanks to homogenous Fenton, heterogeneous Fenton with cathodically adsorbed Fe(III), and electrocatalysis. The mineralization partly corresponded to the gradual destruction of EDDS by hydroxyl radical ($k_{abs} = 5.22\times10^9$ M^{-1} s^{-1}), and involved the formation of 5 oxidation and 6 dimerization or cyclization by-products.

Keywords: Butylated hydroxyanisole; Carbon-felt cathode; Electro-Fenton; Ethylenediamine-*N*,*N*'-disuccinic (EDDS) acid; Water treatment

1. Introduction

In recent years, the electrochemical advanced oxidation processes (EAOPs) based on Fenton's reaction (1) have been investigated in great detail owing to the great ability of the in-situ generated hydroxyl radical ($^{\bullet}OH$) to degrade aqueous organic micropollutants [1-3]. Among them, electro-Fenton (EF) is the most popular method due to its simplicity and easy scalability [4]. Homogeneous EF demands an acidic pH 2.5-3.5 to ensure the total solubilization of Fe(II) or Fe(III) salts, thereby yielding a very fast decontamination.

$$H_2O_2 + Fe(II) \rightarrow Fe(III) + {}^{\bullet}OH + OH^- \quad (1)$$

H_2O_2 is produced on site from the two-electron O_2 reduction reaction (2). Carbonaceous air-diffusion cathodes allow obtaining the highest H_2O_2 concentrations under ambient conditions, hampering any other reduction process [5-8]. Large surface area carbon-felt cathodes generate lower H_2O_2 contents even upon O_2-saturation of solutions [9-11], although they favor the simultaneous Fe(II) regeneration from reaction (3) that maintains the catalytic cycle, thus yielding complete removal of total organic carbon (TOC) [12-15].

$$O_2(g) + 2H^+ + 2e^- \rightarrow H_2O_2 \quad (2)$$

$$Fe(III) + e^- \rightarrow Fe(II) \quad (3)$$

The properties of carbon felt, including high porosity and specific surface area [16,17], make it an optimum choice as three-dimensional electrode. The latest advances on its application to EF treatment and many other electrochemical technologies have been recently reviewed [16,18].

Many industrial effluents and most natural sources of water are at circumneutral pH, which impedes the use of conventional homogeneous EF unless pH regulation and monitoring is carried out. In order to overcome such handicap, heterogeneous EF has been recently developed [19,20], mainly following two different strategies: (i) external addition of suspended iron-based

catalysts [21,22], or (ii) use of iron-based particles supported on substrates like carbonaceous cathodes [23,24] or loaded on membranes and resins [25]. However, the loss of active sites and the lack of stability in consecutive degradation cycles due to iron leaching and gradual solubilization are potential drawbacks.

Lately, a novel alternative has been devised to carry out homogeneous catalytic water treatment operating at mild pH [26]. In particular, ethylenediamine-*N*,*N*′-disuccinic (EDDS) acid has been employed to form the Fe(III)–EDDS complex and catalyze the conventional Fenton-based processes. The performance of this aminopolycarboxylic acid (APCA) has only been tested in non-electrochemical Fenton-like systems, both in the dark [27] and under UV [28] or sunlight irradiation [29]. An electrochemical approach could enhance the continuous electroreduction of Fe(III)–EDDS complex from reaction (3), thus giving rise to a new kind of homogeneous EF process. Note that EDDS is a more suitable ligand than citrate, oxalate and the two most widely used APCAs, nitrilotriacetic (NTA) and ethylenediaminetetraacetic (EDTA) acids, due to its larger biodegradability [27].

Homogeneous catalysis with soluble Fe(III)–EDDS complex can be combined with electrocatalysis by equipping the electrochemical reactor with an anode that is able to produce M(•OH) from water oxidation via reaction (4) [30,31]. Boron-doped diamond (BDD) thin films yield the most active type of M(•OH) but, due to their high cost, dimensionally stable anodes based on RuO_2 or IrO_2 are more commonly employed.

$$M + H_2O \rightarrow M(^{\bullet}OH) + H^+ + e^- \quad (4)$$

In this work, the performance of EF process catalyzed with Fe(III)–EDDS complex to treat butylated hydroxyanisole (BHA) as a model contaminant of emerging concern was thoroughly evaluated. BHA is widely used as food antioxidant and preservative in the cosmetic industry [32], eventually ending in all kinds of water reservoirs. Lately, serious concerns have arisen due to evidences for carcinogenicity [32,33], adverse ecotoxicological effects [34] and its

endocrine disrupting activity [35]. Several authors have studied its degradation by photoassisted methods [36,37], chemical treatments with O_3 [35,37] or chlorine [38], and electrochemical technologies like electrocoagulation as well as conventional EF and photoelectro-Fenton with air-diffusion cathodes and 0.5 mM $FeSO_4$ as catalyst source [39]. Considering the state of the art, the modification of the conventional homogeneous EF process based on EDDS is proposed for the first time. Aqueous solutions with a low BHA concentration and 50 mM Na_2SO_4 at natural pH have been treated in a cell with an IrO_2-based or BDD anode and a carbon-felt cathode, aiming to enhance the Fe(III)–EDDS reduction as a crucial step to produce $^{\bullet}OH$. The operation conditions were optimized from BHA and TOC decays. The contribution of heterogeneous Fenton reaction and the ability of the system for Fe(II) regeneration were assessed from scanning electron microscopy (SEM) with energy dispersive x-ray spectroscopy (EDS), x-ray photoelectron spectroscopy (XPS) and cyclic voltammetry, along with the analysis of the time course of uncomplexed iron species, H_2O_2 and Fe(III)-EDDS complex. A very low Fe(III) concentration was employed in all tests. The steady-state concentration of hydroxyl radicals in the novel system has also been determined. Comparative trials were also performed with a carbon-polytetrafluoroethylene (PTFE) air-diffusion cathode and hydrated Fe^{3+} as catalyst. Reaction by-products were identified by high-performance liquid chromatography (HPLC) and gas chromatography-mass spectrometry (GC-MS), and a degradation mechanism of Fe(III)–EDDS-assisted EF process was finally proposed.

2. Materials and methods

2.1. Chemicals

BHA (99% purity) and *p*-hydroxybenzoic acid (*p*HBA, ≥ 99%) were purchased from Sigma-Aldrich. Na_2SO_4, H_2SO_4, NaOH, $FeSO_4{\cdot}7H_2O$, $FeCl_2$ and $Fe(ClO_4)_3$ of analytical grade were supplied by Merck, J.T. Baker and Sigma-Aldrich. EDDS trisodium salt solution (~ 35%

98 in H_2O) was supplied by Sigma-Aldrich. Ti(IV) oxysulfate for H_2O_2 determination was
99 purchased from Panreac, whereas 1,10-phenantroline monohydrate (99% purity) from Alfa-
100 Aesar and ascorbic acid from Sigma-Aldrich were employed for soluble iron analysis. Organic
101 solvents of HPLC or analytical grade were purchased from Panreac and Merck. All aqueous
102 solutions were prepared with Millipore Milli-Q water (resistivity > 18.2 MΩ cm).

103 The Fe(III)–EDDS complexes with different ratios were formed by mixing appropriate
104 amounts of $Fe(ClO_4)_3$ and EDDS solutions [27] followed by vigorous stirring for 3 min. Stock
105 solutions of 10 mM $Fe(ClO_4)_3$ and EDDS were stored in the dark, and fresh complexes were
106 prepared before each experiment. For example, the combination of each reagent at 0.10 mM
107 gave rise to 0.10 mM Fe(III)–EDDS (1:1) complex. To form the Fe(II)–EDDS complex, $FeCl_2$
108 was used as iron source. In some cases, a sequential addition of Fe(III) and EDDS was followed.
109 Some comparative trials were also performed using $Fe_2(SO_4)_3$ or $FeCl_3$ instead of $Fe(ClO_4)_3$.

110 *2.2. Electrolytic cells*

111 Most of the experiments were carried out in an undivided glass cell thermostated at 25 ºC
112 under stirring with a PTFE follower at 700 rpm. A carbon-felt piece (1.0 cm × 5.0 cm × 0.5 cm)
113 from Mersen was used as cathode. Before first use, it was activated by immersion in a 4 M
114 H_2SO_4 solution at 60 °C for 3 h. The anode of 3 cm^2 geometric area was either an IrO_2-based
115 coated Ti plate purchased from NMT Electrodes or a BDD thin film supplied by NeoCoat. The
116 interelectrode gap was about 1.0 cm. Prior to each electrolysis, compressed air was sparged
117 through the solution at 0.35 mL min^{-1} for 10 min, which was maintained during the trials to
118 ensure the saturation with O_2 for H_2O_2 electrogeneration. After each trial, the cathode was
119 immersed in a 4 M H_2SO_4 solution for 10 min and then rinsed several times with Milli-Q water
120 and dried in an oven at 90 ºC.

121 In some cases, the electrolytic trials were performed with the same cell but replacing the
122 carbon felt by a 3 cm^2 carbon-PTFE air-diffusion electrode supplied by E-TEK, fitted in a

123 tubular gas chamber that was fed with compressed air at 1 L min^{-1}. A preliminary polarization
124 in 100 mL of a 50 mM Na_2SO_4 solution at 300 mA for 180 min allowed the surface cleaning
125 and activation.

126 The electrolytic trials were made with 150 mL of 50 mM Na_2SO_4 solutions, without or with
127 0.076 mM BHA (10 mg L^{-1} TOC).

128 *2.3. Carbon-felt cathode characterization*

129 The morphological features of pristine and Fe(III)-loaded carbon felt were assessed by
130 SEM-EDS employing a field emission scanning electron microscope (JEOL JSM-7100F) at 15
131 kV equipped with an INCA analyzer.

132 XPS analysis was performed with a PHI 5500 Multitechnique System (Physical
133 Electronics) using an Al-Kα monochromatised X-ray source (1486.6 eV and 350 W) placed
134 perpendicularly to the analyzer axis and calibrated using the $3d_{5/2}$ line of Ag (full width at half
135 maximum of 0.8 eV). The analyzed area was a circle of 0.8 mm diameter. The selected
136 resolution for the spectra was 187.85 eV of Pass Energy (PE) and 0.8 eV/step for the general
137 spectra, and 23.5 eV of PE and 0.1 eV/step for the spectra of the different elements. A low
138 energy electron gun (less than 10 eV) was used. All measurements were made under ultra-high
139 vacuum at pressures between 5×10^{-9} and 2×10^{-8} Torr. The spectra were analyzed using the
140 ULVAC-PHI MultiPakTM Software 8.2.

141 The electrochemical characterization was carried out by cyclic voltammetry on an Autolab
142 PGSTAT30 potentiostat. An undivided electrochemical cell containing 50 mL of a 50 mM
143 Na_2SO_4 solution at natural pH and thermostatized at 25 ºC was used. It was equipped with a
144 carbon-felt piece (1.0 cm × 1.0 cm × 0.5 cm), in the absence or presence of pre-adsorbed Fe(III)
145 species, a platinum spiral and Ag|AgCl (KCl sat.) as the working, counter and reference
146 electrode, respectively. The voltammograms were recorded within a potential range from
147 +0.700 V to -1.450 V at a scan rate of 0.100 V s^{-1}. Prior to each run, O_2 was purged out from

148 solutions under a gentle N_2 stream. For comparison, voltammograms were also obtained with a
149 pristine carbon-felt electrode in a 50 mL solution containing 0.10 mM $Fe(ClO_4)_3$ and 50 mM
150 Na_2SO_4 solution at natural pH.

151 *2.4. Other apparatus and analytical methods*

152 Galvanostatic electrolyses were performed with an Amel 2053 potentiostat-galvanostat and
153 the cell voltage (E_{cell}) was provided by a Demestres 601BR digital multimeter. The electrical
154 conductance and pH were measured with a Metrohm 644 conductometer and a Crison GLP 22
155 pH-meter, respectively. Once withdrawn from treated solutions, samples were microfiltered
156 with 0.45 μm PTFE filters from Whatman. H_2O_2 concentration was determined from the light
157 absorption of its yellow Ti(IV) complex, at λ = 408 nm, measured on a Shimadzu 1800 UV/Vis
158 spectrophotometer at 25 °C. The dissolved Fe(II) contents was obtained from the absorbance
159 of their corresponding reddish complex formed with 1,10-phenantroline, at λ = 508 nm. Total
160 dissolved Fe concentration was determined upon addition of ascorbic acid to the previous
161 samples to transform all Fe(III) into Fe(II). Quantitative analysis of Fe was also performed by
162 inductively-coupled plasma with optical detection (ICP-OES) using the Optima 3200L
163 spectrometer from Perkin Elmer. TOC of BHA solutions was determined on a Shimadzu TOC-
164 VCNS analyzer, using the non-purgeable organic content procedure.

165 BHA concentration was analyzed by reversed-phase HPLC using a Waters 600 liquid
166 chromatograph fitted with a BDS Hypersil C18 5 μm, 250 mm × 4.6 mm, column at 35 ºC. It
167 was coupled to a Waters 996 photodiode array detector (PAD) set at 290 nm. The mobile phase
168 was a 70:30 (v/v) CH_3CN/10 mM KH_2PO_4 (pH 3.0) mixture eluted at 0.8 mL min^{-1}, and the
169 peak of BHA was obtained at 5.1 min. Samples were always diluted with CH_3CN to stop the
170 degradation of BHA. The concentration of the Fe(III)–EDDS complex was determined in the
171 same HPLC system, with the PAD set at 240 nm. The mobile phase was a mixture of A and
172 methanol (95:5, v/v), where A was Milli-Q water with 2 mM tetrabutylammonium

hydrogensulfate and 15 mM sodium formate at pH = 4.0, circulating at a flow rate of 0.8 mL min^{-1}. The Fe(III)–EDDS peak was displayed at 10.7 min.

The competition kinetics method with *p*HBA as reference substrate allowed determining of the absolute rate constant (k_{abs}) for the reaction between EDDS and hydroxyl radical, as well as the concentration of this radical. In these experiments, the Fe(III)–EDDS complex was monitored as explained above, whereas a 50:50 (v/v) CH_3CN/H_2O (2% acetic acid) mixture eluted at 1.0 mL min^{-1} was needed to obtain a well defined peak at 3.3 min for *p*HBA. Further details on the methodology can be found elsewhere [40].

Each experiment was performed at least in duplicate and average values are given. The corresponding error bars with 95% confidence interval are given in figures.

GC-MS analysis was performed in a 6890N gas chromatograph (Agilent Technologies) coupled to a 5975C mass spectrometer operating in electron impact mode at 70 eV. A nonpolar Teknokroma Sapiens-X5ms and a polar HP INNOWax column, both of 0.25 μm, 30 m × 0.25 mm, were used. The temperature ramp was: 36 ºC for 1 min, 5 ºC min^{-1} up to 320 ºC, and hold time of 10 min. The temperature of the inlet, source and transfer line was 250, 230 and 300 ºC. Liquid-liquid extractions with CH_2Cl_2 allowed obtaining an organic solution that was further dried over anhydrous Na_2SO_4, filtered and concentrated under reduced pressure. The mass spectra were identified with the NIST05 MS database.

3. Results and discussion

3.1. Comparison of BHA removal with carbon-felt and air-diffusion cathodes

Fig. S1 of Supplementary Material informs about the high stability of the 0.10 mM Fe(III)–EDDS (1:1) complex, regardless of the solution pH between 3.0 and 9.0 (Fig. S1a) or the exposure time to each pH (Fig. S1b-d). Speciation diagrams of ferric complexes as a function of pH determined with solutions containing EDDS showed that the use of this chelating agent

may make Fe(III) soluble until near-neutral pH [41], but here we give an evidence on the stability of the complex even under more alkaline conditions (pH 9.0), which was unexpected.

In Fig. 1, the degradation of 0.076 mM BHA using different iron species at natural pH 5.7 with an IrO_2-based anode and a carbon-felt or air-diffusion cathode, at 50 mA, is depicted. The largest BHA removal was achieved using the carbon-felt cathode (Fig. 1a). In EF with 0.10 mM of either Fe(II)–EDDS (1:1) or Fe(III)–EDDS (1:1) complex, 95%-97% degradation was reached at 45 min. Using Fe(II)–EDDS, the faster BHA decay during the first 10 min can be accounted for by the presence of Fe(II) formed in its complexation equilibria, further yielding $^{\bullet}OH$ from homogeneous Fenton's reaction (1). Conversely, Fe(III)–EDDS is in equilibrium with Fe(III), which promotes the formation of the less powerful hydroperoxyl radical ($HO_2^{\bullet}$) from the following Fenton-like reaction:

$$H_2O_2 + Fe(III) \rightarrow Fe(II) + HO_2^{\bullet} + H^+ \quad (5)$$

Nonetheless, both profiles became very similar with electrolysis time because the interactions between complexed iron and H_2O_2, occurring via homogeneous reactions (6) and (7), are analogous to those from reactions (1) and (5), respectively [27]. Hence, in EF with Fe(II)–EDDS, the organics were mainly degraded by $^{\bullet}OH$ formed from reaction (6), especially during the first minutes. The resulting complex, Fe(III)–EDDS, can be at least partly reduced to Fe(II)–EDDS at the cathode (see below), which explains the quick BHA decay in EF with Fe(III)–EDDS. In addition, this latter complex can yield $HO_2^{\bullet}$ via reaction (7).

$$Fe(II)\text{–}EDDS + H_2O_2 \rightarrow Fe(III)\text{–}EDDS + {}^{\bullet}OH + OH^- \quad (6)$$

$$Fe(III)\text{–}EDDS + H_2O_2 \rightarrow Fe(II)\text{–}EDDS + HO_2^{\bullet} + H^+ \quad (7)$$

Typically, Fe(II) salts are unstable under oxygenated atmosphere owing to gradual oxidation and, moreover, they are more expensive than Fe(III) ones. Since a similar degradation

rate was obtained in both cases, all subsequent assays with EDDS were carried out with the Fe(III) salt.

The BHA decay was much slower in EF with $Fe(ClO_4)_3$ in the absence of EDDS, i.e., conventional homogeneous EF, attaining 60% at 45 min (Fig. 1a). The quick loss of oxidation power from about 10 min can be explained by the partial precipitation of iron as hydroxides/oxides at high pH. Once this occurred, BHA was slowly degraded thanks to: (i) the action of radicals formed from reaction (1) and (5) at a very small content of soluble catalyst, (ii) heterogeneous Fenton's reaction promoted by the solid hydroxides/oxides [19] and, possibly, (iii) adsorption onto solid iron. Note that, despite the iron precipitation, the EF process yielded a faster and larger removal than electro-oxidation with electrogenerated H_2O_2 (EO-H_2O_2). Since blank experiments in the absence of current did not show BHA adsorption on carbon felt, and the absence of ionizable atoms precluded a possible effect of electrosorption, the 44% BHA removal by EO-H_2O_2 at 45 min can be mainly related to the action of $IrO_2(^{\bullet}OH)$ formed via reaction (4). This informs about the much milder action of this radical as compared to homogeneous $^{\bullet}OH$.

Fig. 1b shows the trends obtained with an air-diffusion cathode, which clearly was much less effective than carbon felt to degrade BHA. A very slow disappearance of the pollutant under EO-H_2O_2 conditions can be seen, with a final removal of 13%. It is well known that this cathode possesses an extraordinary ability to generate H_2O_2 [5-8], much greater than carbon felt [9]. Since the H_2O_2 concentration is expected to be much higher than BHA one (= 0.076 mM), $IrO_2(^{\bullet}OH)$ is consumed to a large extent in H_2O_2 oxidation reaction, in contrast to that observed in Fig. 1a. On the other hand, the trend of BHA content in EF without EDDS looks like that commented for Fig. 1a, also attaining a similar decay of 55% at 45 min. As discussed above, in this system most of the iron precipitates and thus, the differences in the reduction power of both cathodes are of minor relevance as compared to heterogeneous reactions and

adsorption on the oxides. Finally, it is worth highlighting the poor BHA degradation in Fe(III)–EDDS-assisted EF, with only 21% removal at 45 min. This behavior can be explained by the insignificant electroreduction of Fe(III)–EDDS on the air-diffusion cathode surface, as will be shown below. Since $^{\bullet}OH$ cannot be formed from reaction (6) and $IrO_2(^{\bullet}OH)$ cannot be accumulated, as shown in EO-H_2O_2, $HO_2^{\bullet}$ constituted the main oxidant. Apart from exhibiting a low oxidation power, the latter radical was greatly consumed in the degradation of EDDS, which competed with BHA.

The effect of the Fe(III) and EDDS dosage using the carbon-felt cathode can be seen in Fig. S2. A faster BHA removal was achieved with 0.20 mM Fe(III)–EDDS (1:1), as compared to 0.10 mM (Fig. 1a), in agreement with a higher amount of Fe(II)–EDDS formed upon cathodic reduction that eventually fostered the production of $^{\bullet}OH$ from reaction (6). Conversely, the decay at 0.40 mM Fe(III)–EDDS was analogous to that at 0.10 mM, which can be justified by the destruction of many $^{\bullet}OH$ during EDDS oxidation. Since all removals at 45 min were close to 95-97%, 0.10 mM was chosen as the optimum concentration in order to keep a low contribution of EDDS to solution TOC.

Some trials were also performed to assess the effect of the Fe(III):EDDS ratio, but 1:2 or higher ratios did not enhance sufficiently the EF performance (not shown). This means that the 1:1 ratio already ensured the total solubilization of 0.10 mM Fe(III) and hence, an excess of EDDS would become detrimental due to the parasitic reactions between $^{\bullet}OH$ and EDDS, decelerating the BHA degradation.

The different time course of key species during the EF process with 0.1 mM Fe(III)–EDDS (1:1) using the carbon-felt or air-diffusion cathode is depicted in Fig. 2. In the absence of BHA, the former cathode allowed the generation of 2.71 mg L^{-1} Fe(II) (i.e., ~ 50% Fe(III) reduction, Fig. 2a) in 10 min, whereupon this content underwent a 8-fold decrease at 45 min. As can be seen in Fig. 2b, this was due to the progressive abatement of EDDS, with 86% removal of

Fe(III)–EDDS complex and the consequent precipitation of iron. In the presence of BHA, Fig. 2b shows that the decomposition of EDDS was somewhat inhibited, as BHA also consumed the •OH, ending in 76% of Fe(III)–EDDS removal. Consequently, the Fe(III) electroreduction was upgraded, with a similar maximum Fe(II) regeneration but undergoing a much slower 2-fold decay thereafter (Fig. 2a). This explains the successful BHA decay during the Fe(III)–EDDS-assisted EF treatment of Fig. 1a. Worth mentioning, suspended iron precipitates were not observed in none of the previous carbon-felt cells, as verified from the clear solutions, which means that the solid iron became rather adsorbed on the cathode surface (as will be explained in subsection 3.2).

The low ability of the air-diffusion cathode to reduce Fe(III) mentioned from Fig. 1b can be verified in Fig. 2a, where a very small concentration of 0.13 mg L^{-1} Fe(II) as maximal was attained throughout all the treatment. This agrees with the aforementioned poor BHA degradation (21%) in this system, which is also confirmed by the slow Fe(III)–EDDS disappearance with 44% removal at 45 min (Fig. 2b). On the other hand, Fig. 2c reveals the extremely low H_2O_2 production in the above cells with carbon felt, reaching 10-13 mg L^{-1} as maximal. This is much lower than 151 mg L^{-1} attained at 45 min with the diffusion cathode, resulting from the highly efficient mass transport of gaseous O_2 to the carbon-PTFE surface.

An additional trial was performed in order to determine the steady-state concentration of hydroxyl radicals in the Fe(III)–EDDS-modified EF process. For this, the experiment shown in Fig. 2 with carbon felt in the absence of BHA was repeated in the presence of *p*HBA. Based on the apparent rate constants obtained for this latter compound and EDDS (Fig. S3), and considering the tabulated value k_{abs}(•OH-*p*-HBA) = 2.19×10^9 M^{-1} s^{-1}, a k_{abs}-value of 5.22×10^9 M^{-1} s^{-1} was calculated for the reaction between EDDS and hydroxyl radicals. This value, along with the apparent rate constant for the disappearance of EDDS alone (determined from Fig. 2b),

yielded a concentration of hydroxyl radicals of 9.5×10^{-12} M, which is close to the values typically reported in conventional homogeneous EF systems [40].

The evolution of Fe(II) concentration over time, using sulfate solutions without BHA, that results from the application of conventional (i.e., without EDDS) and novel (with 0.1 mM Fe(III)–EDDS) EF treatments with carbon-felt cathode at pH 3.0 and natural pH 5.7 is compared in Fig. 3. In the most widespread EF system with carbon felt, performed at the optimum pH 3.0 [9,13,15], 29% of hydrated Fe^{3+} could be reduced at the cathode as maximal, which occurred in only 2 min. An average Fe^{2+} concentration of 1.2 mg L^{-1} remained in solution during the whole electrolysis, ensuring the continuous degradation of BHA mainly by $^{\bullet}OH$ formed from Fenton's reaction (1). Under the same conditions, the presence of EDDS slightly enhanced the Fe(II) regeneration, attaining 34% in 6 min, which can be related to a higher electroactivity of the Fe(III)–EDDS on carbon felt as compared to the hydrated Fe^{3+}. The average Fe^{2+} concentration was 1.3 mg L^{-1}, always higher than in the previous system despite the gradual destruction of EDDS. However, conventional EF seems preferable at pH 3.0, because it performs similarly to novel EF but without TOC increase from EDDS. On the other hand, based on Fig. 3, it is evident that the Fe(III)–EDDS-assisted EF is needed at natural pH. The absence of EDDS led to a poor generation of Fe(II) with a maximal of 0.76 mg L^{-1} in 2 min, which quickly decreased to 0.2 mg L^{-1}, due to immediate precipitation.

The accumulated concentrations of Fe(III) and total dissolved iron during the trials shown in Fig. 3 are depicted in Fig. S4. At pH 3.0, iron was always completely solubilized (i.e., 5.5 mg L^{-1}) along the electrolysis. In addition, a slightly lower amount of Fe(III) was present in solution when the Fe(III)–EDDS complex was used, in agreement with its easier electroreduction to Fe(II) discussed in Fig. 3. At pH 5.7, the absence of EDDS led to a fast decrease of Fe(III) concentration, as occurred with Fe(II), owing to the almost total removal of dissolved iron. On the other hand, at this pH, the larger stability of iron in the presence of EDDS

is confirmed, with total solubilization at time zero, although it gradually disappeared because of EDDS destruction.

The previous experiments were carried out at 50 mA. Trying to enhance the Fe(II) regeneration rate, a higher current of 100 mA was employed. As can be observed in Fig. S5, only a minor enhancement was achieved at 0.1 mM Fe(III)–EDDS (1:1) complex, reaching 3.4 mg L^{-1} as maximal but following a very close profile to the one at 50 mA (Fig. 3). This suggests that the reduction of the Fe(III) complex was accelerated upon current increase, but also the EDDS destruction due to the faster production of $^{\bullet}OH$ from reaction (6). On the other hand, a much greater enhancement of dissolved Fe(II) concentration (i.e., 5.6 mg L^{-1} at 10 min) was feasible operating with 0.2 mM Fe(III)–EDDS (1:1) complex at 100 mA. However, the regeneration efficiency, close to 55%, was only slightly higher than that found at 50 mA, as was discussed from Fig. 2. Furthermore, this was accompanied by the presence of a greater organic matter content in the form of EDDS, which then competed with BHA and its by-products to react with $^{\bullet}OH$.

Once the high performance of the Fe(III)–EDDS-assisted EF process with carbon-felt cathode to degrade BHA in aqueous solutions at its natural pH 5.7 has been demonstrated (Fig. 1a), the possibility of working within a wider pH range of 3.0-9.0 at 50 mA was investigated. Solution pH was monitored during these electrolyses in order to adjust it when needed. As shown in Fig. 4a, it was certainly possible to operate at alkaline pH up to 9.0 since the same BHA decay kinetics as that found at pH 5.7 and 7.0 was maintained, attaining 95% removal at 45 min. Worth noticing in Fig. 4b, almost all the initial iron was kept soluble during the trial at pH 9.0, with only 6% precipitation. This was possible thanks to the greater stability of EDDS at this pH against oxidants as compared to more acid pH values. In contrast, in the absence of EDDS, the almost total (89%) disappearance of dissolved iron can be confirmed in Fig. 4b. Fig. 4a also evidences that the highest degradation rate was achieved at pH 3.0, reaching 100% BHA

344 removal at 20 min. This agrees with the characteristic optimum pH for Fenton's reaction in
345 conventional EF with uncomplexed iron [1,4], which suggests that this value is also optimal for
346 Fenton-like reaction (6).

347 The influence of the applied current on BHA degradation by EF with 0.1 mM Fe(III)–
348 EDDS (1:1) complex at pH 5.7 using the carbon-felt cathode was also studied. Fig. S6
349 highlights the faster and larger pollutant removal as current was increased from 25 to 75 mA,
350 corresponding to abatements from 87% to 100%. This trend cannot be related to the greater
351 Fe(II)–EDDS generation, since it was demonstrated above that current has a minor effect on
352 Fe(III)–EDDS reduction (Fig. S5). Therefore, current mainly determines the H_2O_2
353 concentration produced from reaction (2), which simultaneously affects the $^{\bullet}OH$ amount
354 formed via reaction (6), as well as the $IrO_2(^{\bullet}OH)$ generation rate from reaction (4). Based on
355 the small difference obtained, next trials were made at 50 mA.

356 *3.2. TOC removal and fate of EDDS with carbon-felt cathode*

357 The mineralization ability of the novel Fe(III)–EDDS-assisted process with carbon-felt
358 cathode was assessed under different conditions, using solutions with 23 mg L^{-1} TOC
359 corresponding to 0.076mM BHA (10 mg L^{-1} TOC, i.e., 43% of total TOC) and 0.1 mM EDDS
360 (13 mg L^{-1} TOC, i.e., 57% of total TOC). Fig. 5a shows that the treatment with the IrO_2-based
361 anode was quite ineffective to mineralize the solution. In spite of the almost complete BHA
362 removal achieved with this anode after 45 min (Fig. 1a), only 14% TOC abatement could be
363 reached at 180 min. This means that some of the BHA and EDDS by-products were very
364 refractory to oxidation. This occurred in concomitance with the progressive loss of oxidation
365 power, as can be deduced from Fig. 5b. In 60 min, 90% of the Fe(III)–EDDS complex
366 disappeared from solution, involving the precipitation of iron as explained above. Therefore,
367 from 60 min, the mineralization was pre-eminently caused by $IrO_2(^{\bullet}OH)$ and, maybe,
368 heterogeneous Fenton process (see subsection 3.3). A greater TOC abatement was feasible

when the IrO_2-based anode was replaced by BDD. At pH 5.7, 35% mineralization was attained at 180 min, owing to the high oxidation power of BDD(•OH) that could slowly destroy the very stable intermediates [1,31]. A similar but slightly slower TOC decay was found at pH 9.0, with a final removal of 28%. Nonetheless, the use of BDD at pH 3.0 clearly outperformed the other systems, reaching 71% mineralization, which confirms that this is the optimum pH for Fenton-like reaction (6) that produces •OH, as discussed from Fig. 4 with the IrO_2-base anode. As can be deduced from Fig. 5b, also in the BDD/carbon felt cells the degradation from 60 min was pre-eminently caused by M(•OH), with the potential contribution of heterogeneous Fenton at the precipitated iron species.

E_{cell} values of 7.0 and 8.5 V were recorded during the trials with the IrO_2-based and BDD anodes, respectively. Based on the equation reported elsewhere [4], this gave rise to high energy consumptions of 7.0 and 8.5 kWh m^{-3} at 180 min, as expected from the use of non-optimized reactors operating in batch mode.

In the absence of BHA (i.e., initial TOC of 13 mg L^{-1}), Fig. S7 shows that EDDS could not be practically mineralized by IrO_2(•OH), being reduced by 8% in 180 min. Hence, the 14% TOC abated in Fig. 5a almost exclusively corresponded to BHA transformation into CO_2, whereas the almost total disappearance of Fe(III)–EDDS in Fig. 5b was then accompanied by the transformation of EDDS into intermediates that were unable to complex and solubilize most of the released Fe(III). Conversely, TOC was reduced by 37% employing BDD, thereby generating small organics like carboxylic acids that are hard to become mineralized [4]. Note that the destruction of EDDS under the action of hydroxyl radicals has been reported above, showing a value close to that found by other authors at pH 8.0, i.e., $2.48\pm0.43\times10^9$ M^{-1} s^{-1} [42].

Trying to enhance the TOC removal, some trial was made with addition of EDDS at 30 min, once the Fe(III)–EDDS concentration was only around 0.04 mM. However, a positive effect was not observed, probably because precipitated iron became absorbed on the cathode

and an insignificant amount was released to the solution. Blank experiments showed that carbon felt can adsorb around 80% of solid iron, especially under near-neutral and alkaline conditions.

3.3. Role of the heterogeneous process in Fe(III)–EDDS-assisted EF

Considering the Fe(III)–EDDS-assisted EF process at natural pH 5.7 using the IrO_2-based/carbon felt cell, discussed in previous subsections, BHA removal has been mainly accounted for by the action of $^{\bullet}OH$ formed from Fenton-like reaction (6), whereas TOC abatement was supposed to be caused by $IrO_2(^{\bullet}OH)$. However, it is still unclear if there might be an additional contribution of heterogeneous Fenton reaction in this novel system. To study this, the treatment of BHA solution as in Fig. 1a with 0.10 mM Fe(III)–EDDS (i.e., simultaneous addition of both reagents), but at pH 9.0, was compared with a sequential addition. The former approach allowed working with the soluble complex, whereas precipitation of iron species, either complexed (≡Fe(III)–EDDS) or uncomplexed (≡Fe) on the cathode surface (≡), was presumed in the latter case (Fig. S8a). As can be seen in Fig. S8b, a very low iron content below 1 mg L^{-1} was determined in solution during the sequential addition (see inset). Nevertheless, the degradation of BHA was very effective, with an analogous profile to that obtained following a simultaneous addition. Heterogeneous reaction was thus believed to be a crucial mechanism in the absence of sufficient amount of soluble Fe(III)–EDDS, which is exactly what occurs as EDDS becomes degraded, as stated above. On the other hand, the contribution of heterogeneous Fenton to TOC removal was insignificant (Fig. S8c).

The existence of such precipitates on the cathode surface was verified via SEM-EDS analysis. The images in Fig. 6a-c depict the morphology of pristine carbon felt at different magnifications. Smooth carbon fibers with only random effects arisen upon activation in acid medium can be observed. The EDS analysis of Fig. 6d confirms the high purity of this material before use. Then, the sequential procedure described above at pH 9.0 (Fig. S8a) was followed to load the fibers with solid iron and/or iron–EDDS, although using higher concentrations of

419 $Fe(ClO_4)_3$ and EDDS aiming to enhance the formation of precipitates and facilitate the analysis.
420 Fig. 6e-g perfectly illustrate the presence of iron precipitates on carbon fibers, dispersed
421 throughout the whole volume of the sample and showing good attachment. Fig. 6h confirms the
422 presence of iron and oxygen in those particles, alongside sodium and sulfur from the
423 background electrolyte employed during the precipitation.

424 XPS analysis of iron-loaded carbon felt, once employed as cathode in the IrO_2-
425 based/carbon felt cell at 50 mA for 10 min, was made in order to elucidate the nature of the iron
426 particles. In the spectrum of Fig. 7, it is very interesting to notice the existence of ≡Fe(II), which
427 logically arouse during the short electrolyses made with the modified carbon-felt cathode, along
428 with ≡Fe(III). The existence of mixed oxide particles like Fe_3O_4 cannot be discarded either to
429 explain the presence of ≡Fe(II). Main peaks located at 711.2 and 713.4 eV for Fe(II) and Fe(III)
430 in the Fe $2p_{3/2}$ region were detected, in addition to peaks at 724.6 and 726.8 eV for Fe(II) and
431 Fe(III) in the Fe $2p_{1/2}$ region, respectively, consistent with previously reported spectra for iron-
432 loaded carbonaceous materials [43,44]. In addition, two satellite peaks appeared at 717.6 and
433 720.9 eV. Two analogous experiments were performed employing either $FeCl_3$ or $Fe_2(SO_4)_3$ as
434 Fe(III) source, instead of $Fe(ClO_4)_3$, aiming to assess any possible influence on the performance
435 of the novel EF process. However, no substantial peak shifts were observed, as shown in Fig.
436 S9. For $FeCl_3$ (Fig. S9a), the peaks appeared at 711.1 and 712.9 eV for Fe(II) and Fe(III) in the
437 Fe $2p_{3/2}$ region, and 724.5 and 726.8 eV in the Fe $2p_{1/2}$ region. Using $Fe_2(SO_4)_3$ (Fig. S9b), the
438 values were practically the same, with a difference of 0.1 eV as maximum.

439 Once confirmed the occurrence of heterogeneous Fenton process in the Fe(III)–EDDS-
440 assisted treatment, resulting from the precipitation of iron-based particles on the carbon-felt
441 cathode surface, the redox activity of this solid iron was assessed by cyclic voltammetry. A
442 small piece of carbon felt was loaded with iron species as described in Fig. S8, but using 0.10
443 mM of each reagent to work in the same conditions employed for BHA degradation. A blank

voltammogram was recorded on pristine carbon felt, immersed into 50 mL of a 50 mM Na_2SO_4 solution at natural pH. No peaks appeared over the potential range from +0.700 V to -1.450, as evidenced in Fig. 8. In contrast, with the modified working electrode, a quasi-reversible adsorption signal related with ≡Fe(III) to ≡Fe(II) (R, reduction peak) and ≡Fe(II) to ≡Fe(III) (O, oxidation peak) transformations was observed. The cathodic and anodic peak potential values appeared at E_p^c = -0.815 V vs. Ag|AgCl and E_p^a = -0.277 V vs. Ag|AgCl, respectively, yielding ΔE_p = 0.538 V. These peaks were very similar to those found in a voltammetric study with 0.10 mM $Fe(ClO_4)_3$ in a 50 mM Na_2SO_4 solution (Fig. S10), with E_p^c = -0.775 V vs. Ag|AgCl and E_p^a = -0.333 V vs. Ag|AgCl.

The aforementioned results allow concluding that the application of constant current in the novel EF treatment promotes at least the partial transformation of ≡Fe(III) (and/or ≡Fe(III)–EDDS) into ≡Fe(II) (and/or ≡Fe(II)–EDDS). From data obtained in Fig. 8, the half-wave potential ($E_{1/2}$) value of Fe(III –EDDS/Fe(II)–EDDS was calculated as -0.316 V vs the standard hydrogen electrode (SHE). Other authors reported $E_{1/2}$ values of 0.186 V vs SHE at pH 7.0 [45] and 0.069 V vs SHE at pH 6.2 [27], in both cases on glassy carbon.

3.4. Reaction pathways and degradation mechanism

Based on the eleven primary aromatic by-products identified by GC-MS analysis, two different reaction pathways are proposed in Fig. 9 to explain the degradation of BHA (**1**) by the novel homogeneous EF process with Fe(III)–EDDS as catalyst and carbon felt as cathode.

Five by-products were formed through the oxidation route of **1** promoted by •OH or M(•OH). First, **1** was oxidized to either 3-*tert*-butyl-5-methoxybenzene-1,2-diol (**2**), also called 3-*tert*-butyl-4,5-dihydroxyanisole, or 2-*tert*-butylhydroquinone (**3**). The latter was then easily transformed into 2-*tert*-butyl-1,4-benzoquinone (**4**), since the oxidation of hydroquinones to benzoquinones is easily promoted in oxidizing media. Alternatively, the loss of the *tert*-butyl group of **3** yielded hydroquinone (**5**), which again was readily oxidized to *p*-benzoquinone (**6**).

Note that compound **2** was also formed upon the action of O_3 and $S_2O_8^{2-}$ [36,37], whereas compound **3** is a typical metabolite in aqueous media and some authors has explained its formation by demethylation of the methoxy group of **1** [46]. Compound **3** has been reported during biological degradation, UV photolysis [47] and chlorination [38] of BHA. The conversion of **3** into **4** was also reported elsewhere [36-38,47].

The formation of the other six by-products involved dimerization and/or cyclization steps. Dimerization of **1** yielded 3,3'-di-*tert*-butyl-5,5'-dimethoxy-biphenyl-2,2'-diol (**7**), as also reported by Lau et al. [36,37]. This by-product could be transformed into bicyclohexyl-3,6,3',6'-tetraene-2,5,2',5'-tetraone (**8**) upon loss of both *tert*-butyl groups and complete oxidation of the four oxygenated groups. A similar product was found by some authors, but keeping the *tert*-butyl groups in the structure [36,37]. Alternatively, the dimer **7** could yield **9** thanks to cyclization and oxidation. This latter compound could also appear from reaction between **1** with **2**, followed by cyclization and oxidation. Subsequent loss of both methoxy groups of **9** alongside internal rearrangement justifies the formation of 2,6-di-*tert*-butyl-1H-dibenzofuran-4-one (**10**), which is similar to BHDQ in Lau et al. [36,37]. The formation of benzofuran derivative **11** is connected to the oxidation route describe above, since it can arise from internal cyclization of **3**. Finally, compound **12** can be explained by the loss of *ter*t-butyl group of **1** and attack of the –OH group on another aromatic derivative of BHA.

Based on the large set of results summarized in this work, the degradation mechanism shown in Fig. 10 aims at explaining the performance of Fe(III)–EDDS-assisted EF process at circumneutral pH. For simplicity, hydrated Fe^{2+} and Fe^{3+} present in solution are also represented as Fe(II) and Fe(III). The carbon-felt surface allowed: (i) the two-electron reduction of O_2 to H_2O_2 via reaction (2), (ii) the reduction of dissolved Fe(III) and Fe(III)–EDDS, to yield uncomplexed and complexed Fe(II), respectively, which led to the formation of $^{\bullet}OH$ from reaction (6) and (iii) the reduction of adsorbed ≡Fe(III) and ≡Fe(III)–EDDS to yield ≡Fe(II) and

494 ≡Fe(II)–EDDS. These four species gave rise to heterogeneous Fenton and Fenton-like reactions,
495 which yielded •OH and HO_2•, respectively. Therefore, BHA was degraded by •OH formed from
496 those reactions, in concomitance with M(•OH) formed at the anode surface via reaction (4). In
497 addition, it could undergo direct anodic oxidation, as depicted in Fig. 10. On the other hand,
498 both kinds of radicals were responsible for the destruction of EDDS in the Fe(II)–EDDS and
499 Fe(III)–EDDS complexes.

500 **4. Conclusions**

501 Fe(III)–EDDS-modified EF has been proven a very effective process for the removal of
502 aromatic pollutants like BHA at mild pH. Carbon felt outperformed the air-diffusion cathode to
503 run this process, despite the much lower H_2O_2 electrogeneration, because it allowed the
504 regeneration of Fe(II). This species, either uncomplexed or complexed with EDDS, promoted
505 the formation of •OH from classical Fenton's reaction and alternative Fenton-like reaction. A
506 much higher Fe(III) reduction efficiency was observed in the novel Fe(III)–EDDS-assisted EF
507 process as compared to conventional EF with hydrated Fe^{3+}. The optimum pH for Fenton-like
508 reaction between Fe(III)–EDDS and H_2O_2 was 3.0, which agrees with that of conventional
509 Fenton's reaction. The contribution to total TOC and the scavenging effect of EDDS on •OH
510 are the main concerns, preventing the occurrence of a large mineralization. The use of a high
511 oxidation power anode like BDD and solution acidification to pH 3.0 led to 71% TOC
512 abatement after 180 min at 50 mA. Eleven aromatic by-products were identified during the
513 mineralization of BHA. As revealed by SEM-EDS, XPS and voltammetric analyses, the
514 degradation mechanism included homogeneous Fenton's reaction in the bulk solution,
515 heterogeneous Fenton at the cathode surface and electrocatalysis at the anode surface. This new
516 approach to EF treatment is environmental friendly, being very promising for management of
517 water containing persistent organic pollutants.

Acknowledgments

The authors thank financial support from project CTQ2016-78616-R (AEI/FEDER, EU) and PhD scholarship awarded to Z.H. Ye (State Scholarship Fund, CSC, China).

References

[1] I. Sirés, E. Brillas, M.A. Oturan, M.A. Rodrigo, M. Panizza, Environ. Sci. Pollut. Res. 21 (2014) 8336-8367.

[2] C.A. Martínez-Huitle, M.A. Rodrigo, I. Sirés, O. Scialdone, Chem. Rev. 115 (2015) 13362-13407.

[3] J. Radjenovic, D.L. Sedlak, Environ. Sci. Technol. 49 (2015) 11292-11302.

[4] E. Brillas, I. Sirés, M.A. Oturan, Chem. Rev. 109 (2009) 6570-6631.

[5] A. Galia, S. Lanzalaco, M.A. Sabatino, C. Dispenza, O. Scialdone, I. Sirés, Electrochem. Commun. 62 (2016) 64-68.

[6] S. Lanzalaco, I. Sirés, M.A. Sabatino, C. Dispenza, O. Scialdone, A. Galia, Electrochim. Acta 246 (2017) 812-822.

[7] G. Coria, T. Pérez, I. Sirés, E. Brillas, J.L. Nava, Chemosphere 198 (2018) 174-181.

[8] J.R. Steter, E. Brillas, I. Sirés, Appl. Catal. B: Environ. 224 (2018) 410-418.

[9] I. Sirés, J.A. Garrido, R.M. Rodríguez, E. Brillas, N. Oturan, M.A. Oturan, Appl. Catal. B: Environ. 72 (2007) 382-394.

[10] E. Isarain-Chávez, P.L. Cabot, F. Centellas, R.M. Rodríguez, C. Arias, J.A. Garrido, E. Brillas, J. Hazard. Mater. 185 (2011) 1228-1235.

[11] E. Isarain-Chávez, R.M. Rodríguez, P.L. Cabot, F. Centellas, C. Arias, J.A. Garrido, E. Brillas, Water Res. 45 (2011) 4119-4130.

[12] M. Zhou, Q. Tan, Q. Wang, Y. Jiao, N. Oturan, M.A. Oturan, J. Hazard. Mater. 215-216 (2012) 287-293.

[13] A. Dirany, I. Sirés, N. Oturan, A. Özcan, M.A. Oturan, Environ. Sci. Technol. 46 (2012) 4074-4082.

[14] F. Yu, M. Zhou, X. Yu, Electrochim. Acta 163 (2015) 182-189.

[15] O. Ganzenko, N. Oturan, I. Sirés, D. Huguenot, E.D. van Hullebusch, G. Esposito, M.A. Oturan, Environ. Chem. Lett. 16 (2018) 281-286.

[16] J. González-García, P. Bonete, E. Expósito, V. Montiel, A. Aldaz, R. Torregrosa-Macià, J. Mater. Chem. 9 (1999) 419-426.

[17] L.F. Castañeda, F.C. Walsh, J.L. Nava, C. Ponce de León, Electrochim. Acta 258 (2017) 1115-1139.

[18] T.X.H. Le, M. Bechelany, M. Cretin, Advances in carbon felt for electro-Fenton process, in: M. Zhou, M.A. Oturan, I. Sirés (Eds.), Electro-Fenton Process: New Trends and Scale-Up, Springer Nature, Singapore, 2018, pp. 145-173.

[19] S.O. Ganiyu, M. Zhou, C.A. Martínez-Huitle, Appl. Catal. B: Environ. 235 (2018) 103-129.

[20] P.V. Nidheesh, H. Olvera-Vargas, N. Oturan, M.A. Oturan, Heterogeneous electro-Fenton process: Principles and applications, in: M. Zhou, M.A. Oturan, I. Sirés (Eds.), Electro-Fenton Process: New Trends and Scale-Up, Springer Nature, Singapore, 2018, pp. 85-110.

[21] C. Zhang, M. Zhou, G. Ren, X. Yu, L. Ma, J. Yang, F. Yu, Water Res. 70 (2015) 414-424.

[22] C. Zhang, M. Zhou, X. Yu, L. Ma, F. Yu, Electrochim. Acta 160 (2015) 254-262.

[23] Q. Peng, H. Zhao, L. Qian, Y. Wang, G. Zhao, Appl. Catal. B: Environ. 174-175 (2015) 157-166.

[24] Z. Ai, T. Mei, J. Liu, J. Li, F. Jia, L. Zhang, J. Qiu, J. Phys. Chem. C 111 (2017) 14799-14803.

[25] D. Fernández, I. Robles, F.J. Rodríguez-Valadez, L.A. Godínez, Chemosphere 199 (2018) 251-255.

[26] N. Wang, T. Zheng, G. Zhang, P. Wang, J. Environ. Chem. Eng. 4 (2016) 762-787.

[27] W. Huang, M. Brigante, F. Wu, C. Mousty, K. Hanna, G. Mailhot, Environ. Sci. Technol. 47 (2013) 1952-1959.

[28] J. Li, G. Mailhot, F. Wu, N. Deng, J. Photochem. Photobiol. A: Chem. 212 (2010) 1-7.

[29] P. Soriano-Molina, J.L. García-Sánchez, O.M. Alfano, L.O. Conte, S. Malato, J.A. Sánchez-Pérez, Appl. Catal. B: Environ. 233 (2018) 234-242.

[30] B. Marselli, J. García-Gomez, P.A. Michaud, M.A. Rodrigo, C. Comninellis, J. Electrochem. Soc. 150 (2003) D79-D83.

[31] M. Panizza, G. Cerisola, Chem. Rev. 109 (2009) 6541-6569.

[32] H. Verhagen, P.A.E.L. Schilderman, J.C.S. Kleinjans, Chemico-Biol. Interact. 80(2) (1991) 109-134.

[33] F. Shahidi, P. Ambigaipalan, J. Funct. Foods 18B (2015) 820-897.

[34] A. Jos, G. Repetto, J.C. Ríos, A. del Peso, M. Salguero, M.J. Hazen, M.L. Molero, P. Hernández-Freire, J.M. Pérez-Martín, V. Labrador, A. Cameán, Aquat. Toxicol. 71(2) (2005) 183-192.

[35] W. Chu, T.K. Lau, J. Hazard. Mater. 144 (2007) 249-254.

[36] T.K. Lau, W. Chu, N.J.D. Graham, Environ. Sci. Technol. 41 (2007) 613-619.

[37] T.K. Lau, W. Chu, N. Graham, Water Res. 41 (2007) 765-774.

[38] R. Rodil, J.B. Quintana, R. Cela, J. Hazard. Mater. 199-200 (2012) 73-81.

[39] Z. Ye, E. Brillas, F. Centellas, P.L. Cabot, I. Sirés, Sep. Purif. Technol. 208 (2019) 19-26.

[40] I. Sirés, E. Guivarch, N. Oturan, M.A. Oturan, Chemosphere 72 (2008) 592-600.

[41] L. Clarizia, D. Russo, I. Di Somma, R. Marotta, A. Andreozzi, Appl. Catal. B: Environ. 209 (2017) 358-371.

[42] Y. Zhang, N. Klamerth, P. Chelme-Ayala, M.G. El-Din, Environ. Sci. Technol. 50 (2016) 10535-10544.

[43] D. Zhou, L. Yang, L. Yu, J. Kong, X. Yao, W. Liu, Z. Xu, X. Lu, Nanoscale 7 (2015) 1501-1509.

[44] Y.-L. Liu, X.-Y. Xu, C.-X. Shi, X.-W. Ye, P.-C. Sun, T.-H. Chen, RSC Adv. 7 (2017) 8879-8885.

[45] Y. Zhang, N. Klamerth, S.A. Messele, P. Chelme-Ayala, M.G. El-Din, J. Hazard. Mater. 318 (2016) 371-378.

[46] R. Rodil, J.B. Quintana, G. Basaglia, M.C. Pietrogrande, R. Cela, J. Chromatogr. A 1217 (2010) 6428-6435.

[47] G. Alvarez-Rivera, M. Llompart, C. Garcia-Jares, M. Lores, J. Chromatogr. A 1390 (2015) 1-12.

606 **Figure captions**

607 **Fig. 1**. Time course of the normalized BHA concentration decay during the treatment of 150
608 mL of 0.076 mM BHA solutions with 50 mM Na_2SO_4 at natural pH 5.7 and 50 mA by: (△,▲)
609 EO-H_2O_2, (□,■) conventional homogeneous EF with 0.10 mM $Fe(ClO_4)_3$, and novel
610 homogeneous EF with 0.10 mM (○,●) Fe(III)–EDDS (1:1) or (◇) Fe(II)–EDDS (1:1)
611 complex, using a 3-cm^2 IrO_2-based anode and a (a) carbon-felt (1.0 cm × 5.0 cm × 0.5 cm) or
612 (b) 3-cm^2 carbon-PTFE air-diffusion cathode.

613 **Fig. 2.** Change of (a) Fe(II), (b) normalized Fe(III)–EDDS and (c) accumulated H_2O_2
614 concentrations with electrolysis time during the novel EF treatment of 150 mL of 50 mM
615 Na_2SO_4 solutions (▽,▼) without and (○) with 0.076 mM BHA at natural pH 5.7 and 50 mA
616 using an IrO_2-based anode and a (▽,○) carbon-felt or (▼) air-diffusion cathode, with 0.10 mM
617 Fe(III)–EDDS (1:1) complex.

618 **Fig. 3.** Time course of Fe(II) concentration during the treatment of 150 mL of 50 mM Na_2SO_4
619 solutions at 50 mA by (△,□) conventional homogeneous EF with 0.10 mM $Fe(ClO_4)_3$ or (▽,
620 ◇) novel homogeneous EF with 0.10 mM Fe(III)–EDDS (1:1) complex, at (△,▽) natural pH
621 and (□,◇) pH 3.0 using an IrO_2-based anode and a carbon-felt cathode.

622 **Fig. 4.** (a) Normalized BHA concentration decay with electrolysis time during the treatment of
623 150 mL of 0.076 mM BHA solutions with 50 mM Na_2SO_4 at 50 mA by the novel homogeneous
624 EF with 0.10 mM Fe(III)–EDDS (1:1) complex, using an IrO_2-based anode and a carbon-felt
625 cathode. Initial pH: (△) 3.0, (○) 5.7 (natural), (▽) 7.0 and (◇) 9.0. (b) Change of dissolved
626 iron concentration under the conditions of plot (a) at pH 9.0, as compared to that found in the
627 absence of EDDS.

628 **Fig. 5.** Abatement of (a) normalized TOC and (b) Fe(III)–EDDS concentration with electrolysis
629 time during the treatment of 150 mL of 0.076 mM BHA (10 mg L^{-1} TOC) solutions with 50
630 mM Na_2SO_4 at 50 mA by the novel homogeneous EF with 0.10 mM Fe(III)–EDDS (1:1)
631 complex, using a (▲,●,◆) BDD or (○) IrO_2-based anode and a carbon-felt cathode. Initial
632 pH: (▲) 3.0, (●,○) 5.7 (natural) and (◆) 9.0.

633 **Fig. 6.** Scanning electron micrographies at 200×, 500× and 5000× of: (a, b, c) pristine carbon
634 felt (1.0 cm × 5.0 cm × 0.5 cm), and (e, f, g) carbon felt (1.0 cm × 5.0 cm × 0.5 cm) loaded with
635 Fe(III) by following a sequential addition of 1 mM $Fe(ClO_4)_3$ and 1 mM EDDS in 150 mL of a
636 50 mM Na_2SO_4 solution at pH 9.0, maintaining a vigorous stirring for 15 min. (d, h) EDS
637 analyses of the two samples.

638 **Fig. 7.** XPS spectrum of Fe(III)-loaded carbon felt after 10 min of electrolysis at 50 mA using
639 an IrO_2-based anode. The loading was made as described in Fig. 6.

640 **Fig. 8.** Cyclic voltammograms recorded for a carbon-felt electrode (1.0 cm × 1.0 cm × 0.5 cm),
641 in the (dashed line) absence and (solid line) presence of pre-adsorbed Fe(III) species, in 50 mL
642 of 50 mM Na_2SO_4 solutions at natural pH and 25 ºC. Initial and final potential: 0.700 V, reversal
643 potential: -1.450 V. Scan rate: 0.100 V s^{-1}.

644 **Fig. 9.** Reaction pathways for BHA (**1**) degradation by the novel homogeneous EF process with
645 0.10 mM Fe(III)–EDDS (1:1) complex using an IrO_2-based anode and a carbon-felt cathode at
646 circumneutral pH. The main oxidants are M(•OH) formed at the anode surface from water
647 oxidation and/or •OH in the bulk from Fenton's reaction (1) and Fenton-like reaction (6).

648 **Fig. 10.** Proposed mechanism for Fe(III)–EDDS-assisted EF treatment at circumneutral pH.
649

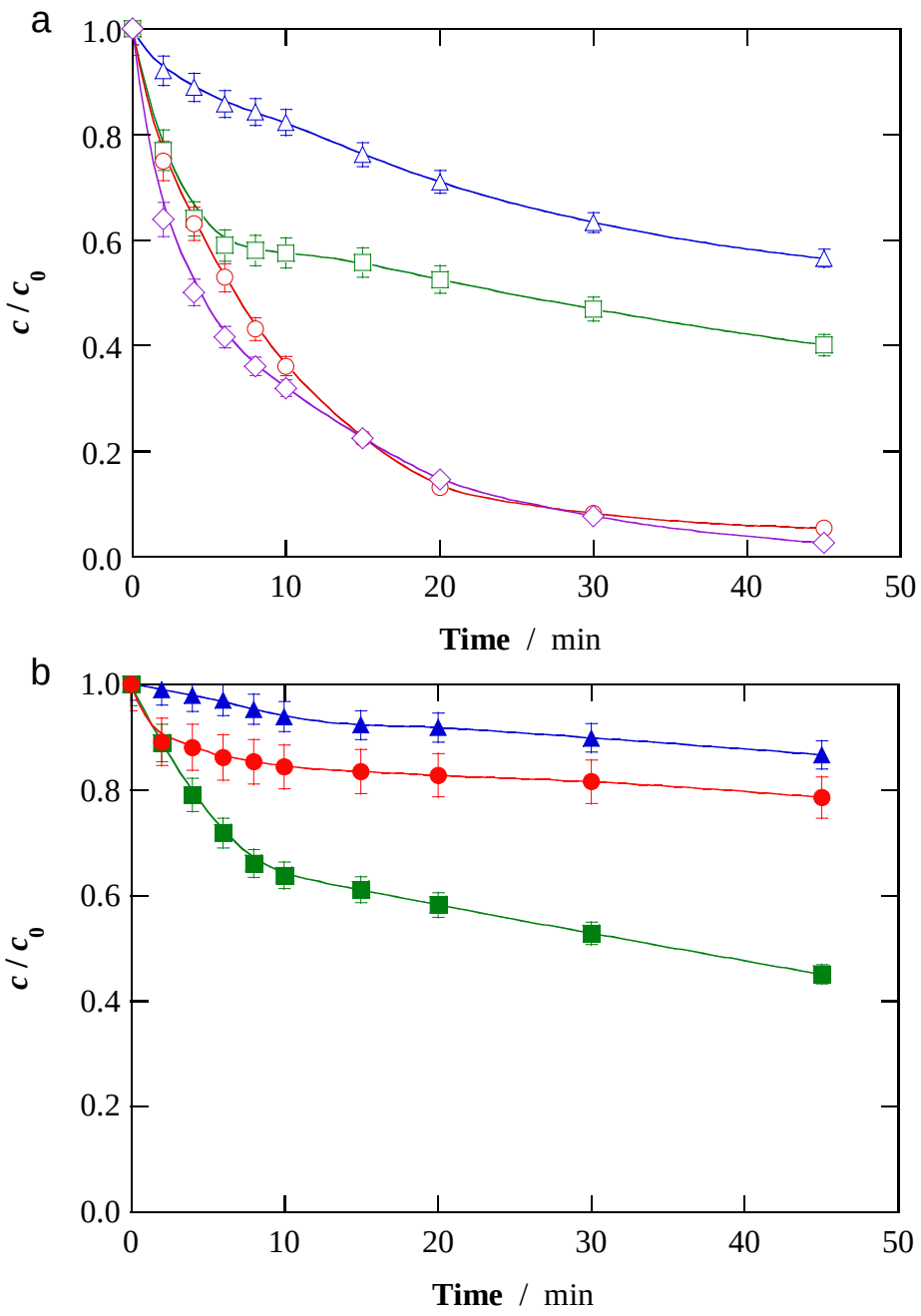
a
1.0
0.8
0.6
0.4
0.2
0.0
c / c0
0
10
20
30
40
50
Time / min
b
1.0
0.8
0.6
0.4
0.2
0.0
c / c0
0
10
20
30
40
50
Time / min

Fig. 1

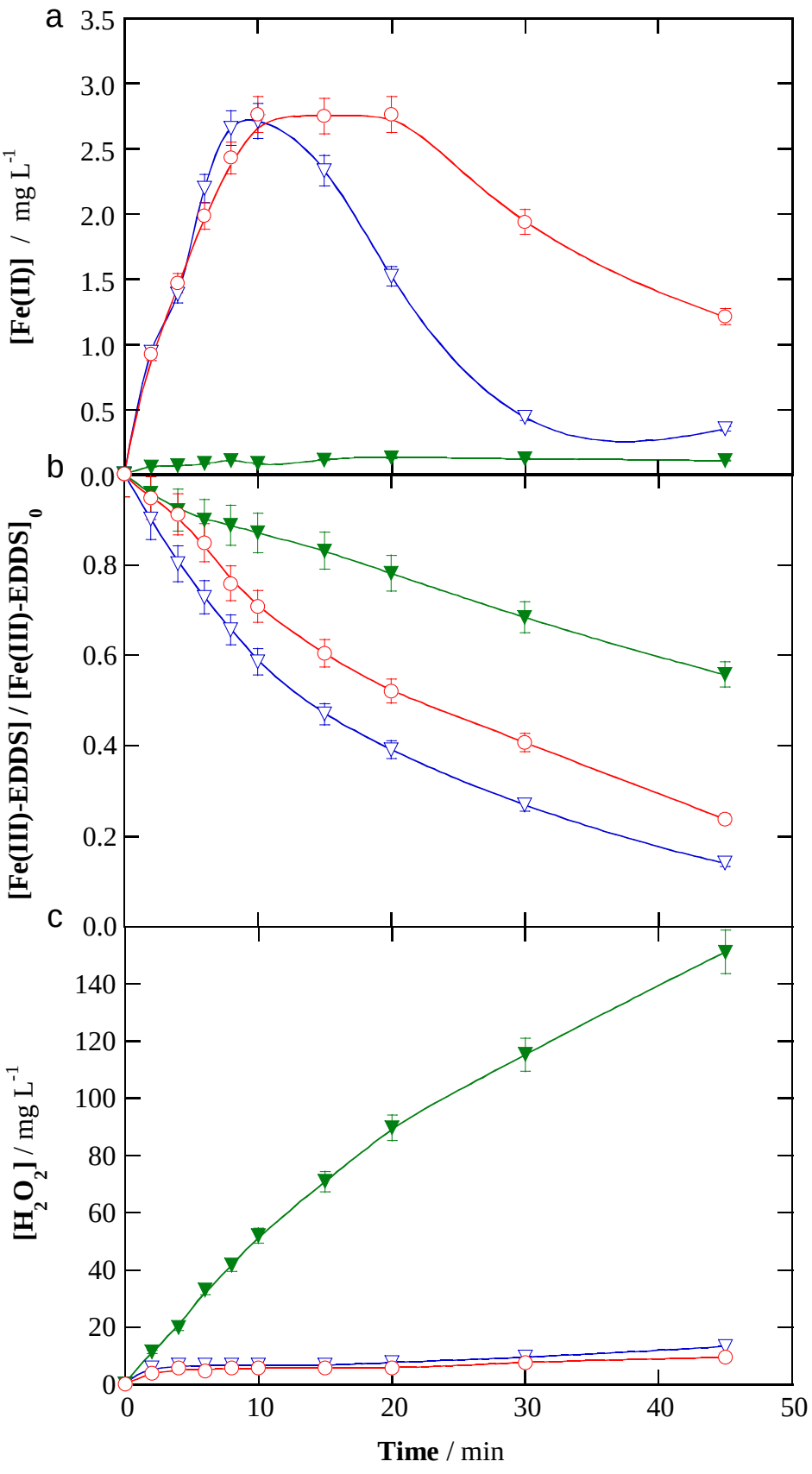
a
b
c
[Fe(II)] / mg L-1
[Fe(III)-EDDS] / [Fe(III)-EDDS]0
[H2O2] / mg L-1
Time / min
0
10
20
30
40
50
0.0
0.5
1.0
1.5
2.0
2.5
3.0
3.5
0.2
0.4
0.6
0.8
0
20
40
60
80
100
120
140

Fig. 2

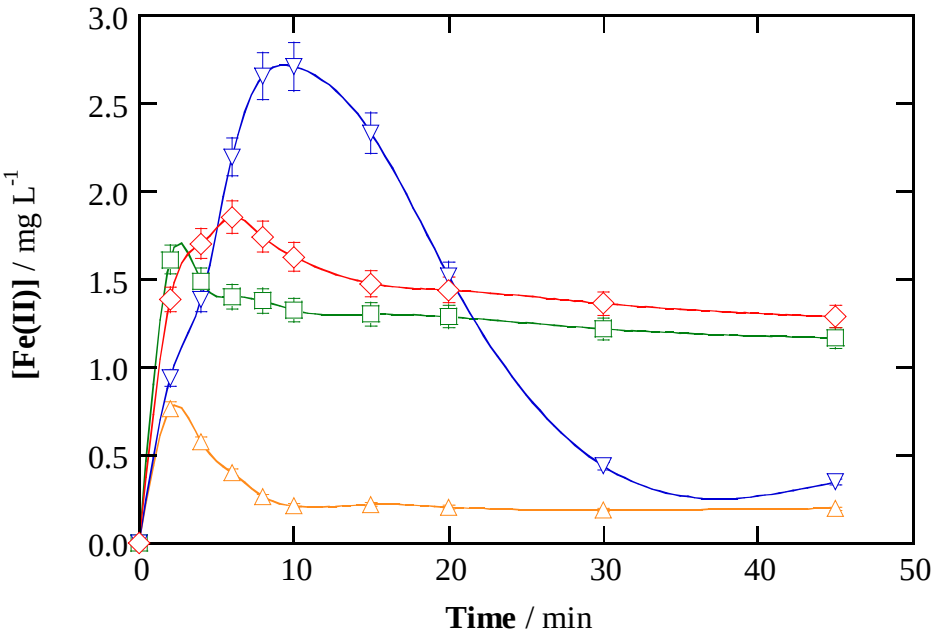

Fig. 3

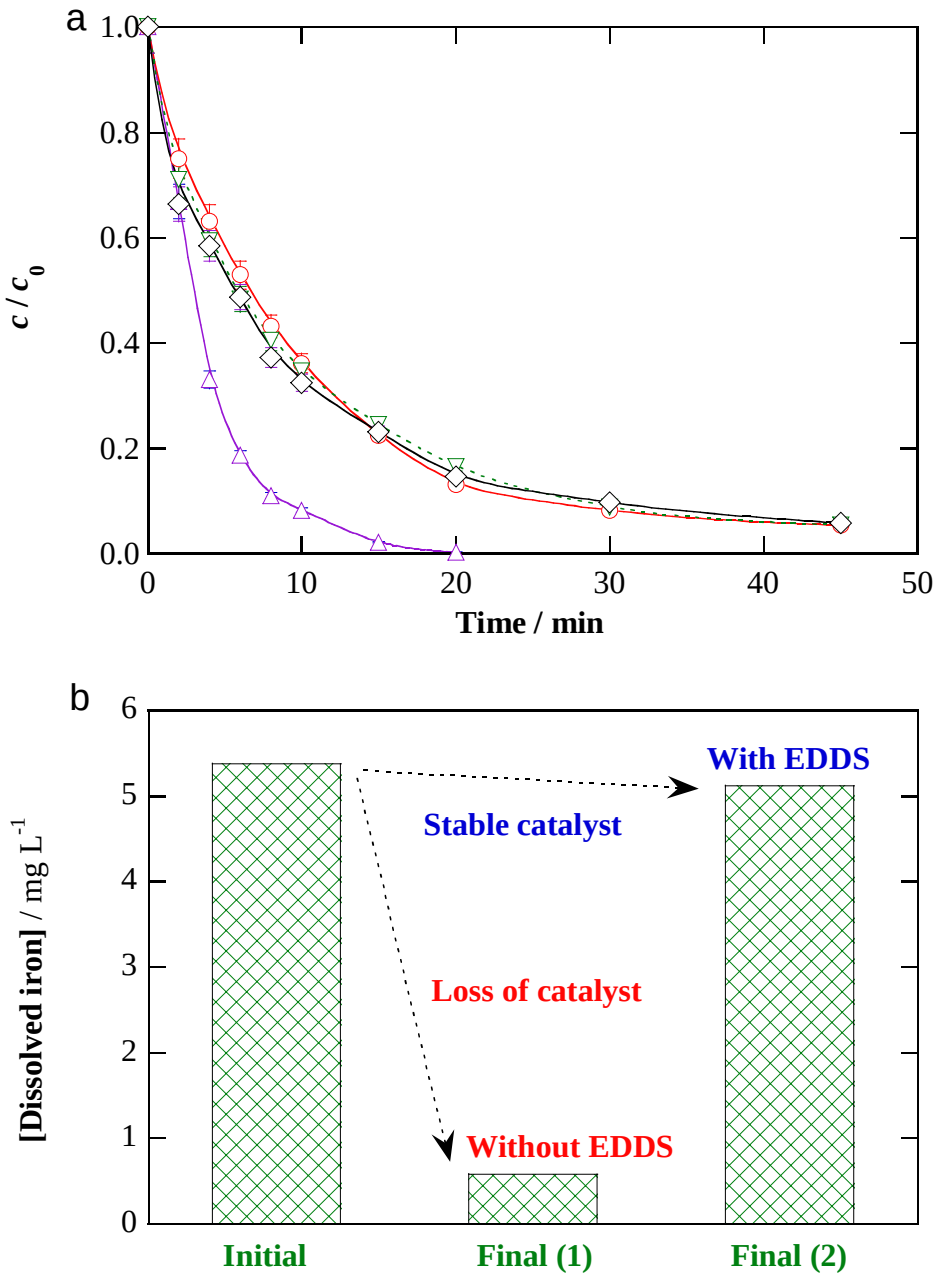
a
1.0
0.8
0.6
0.4
0.2
0.0
c / c0
0
10
20
30
40
50
Time / min
b
6
5
4
3
2
1
0
[Dissolved iron] / mg L-1
With EDDS
Stable catalyst
Loss of catalyst
Without EDDS
Initial
Final (1)
Final (2)

Fig. 4

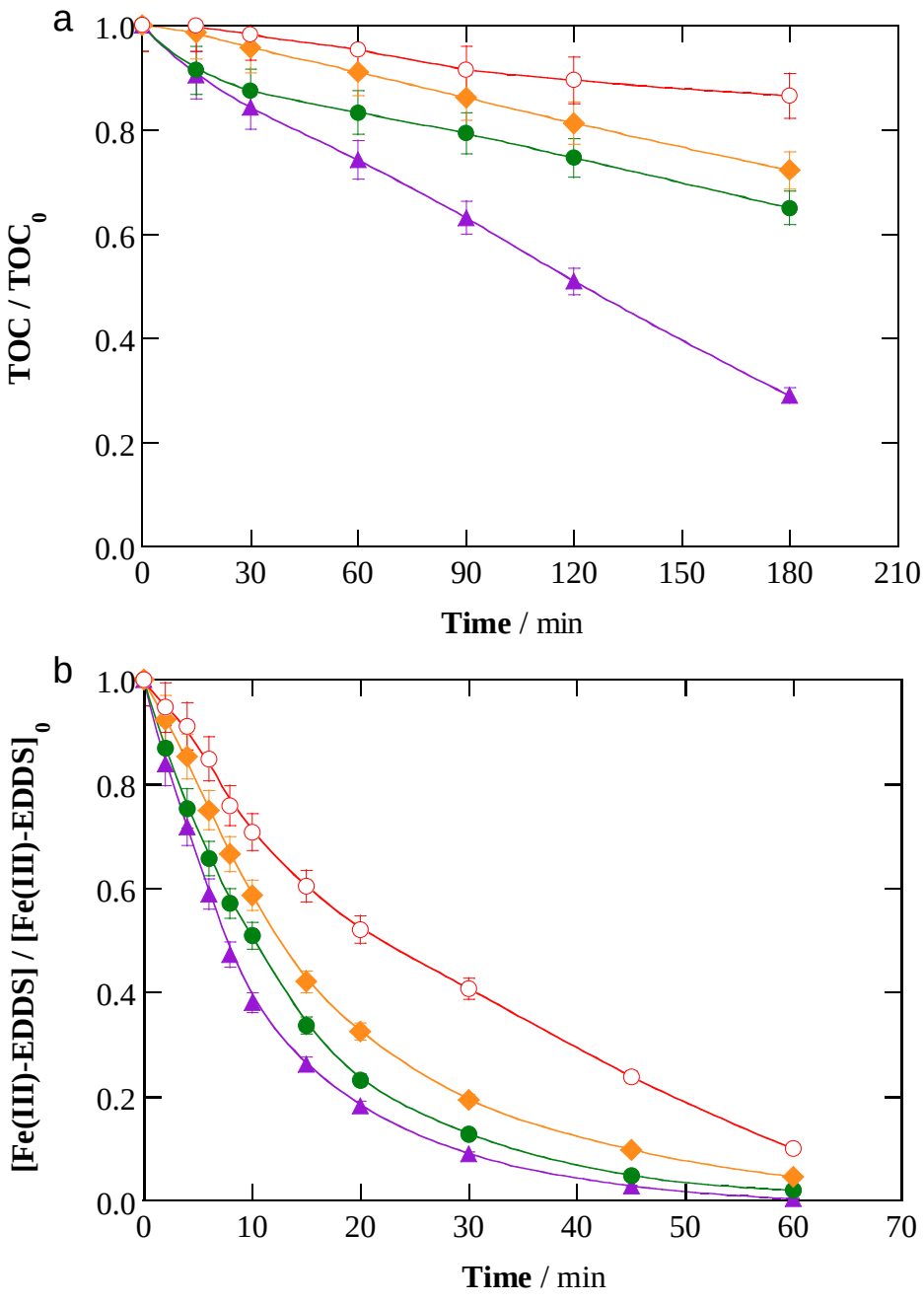

Fig. 5

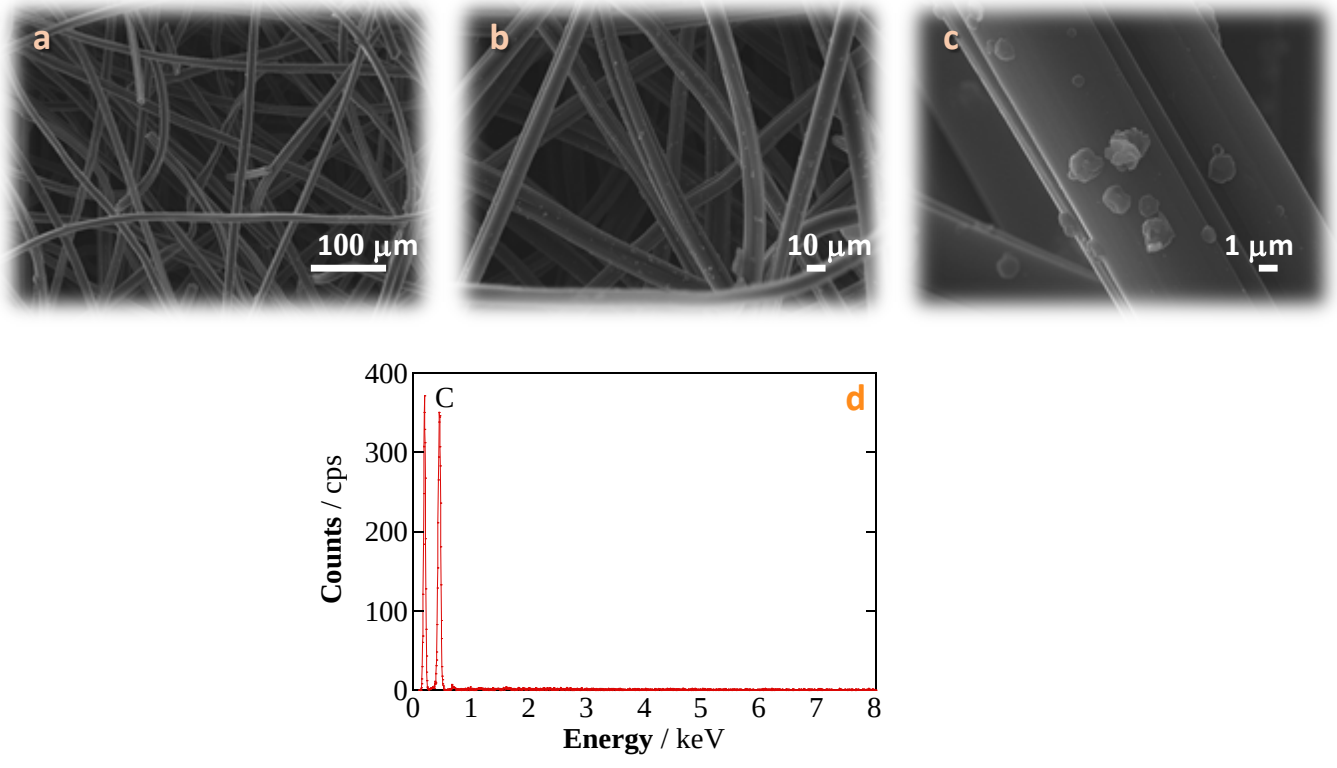
a
100 µm
b
10 µm
c
1 µm
d
C
Counts / cps
Energy / keV
e
100 µm
f
10 µm
g
1 µm
h
S
Na
O
C
Fe
S
Fe
Fe
Counts / cps
Energy / keV

Fig. 6

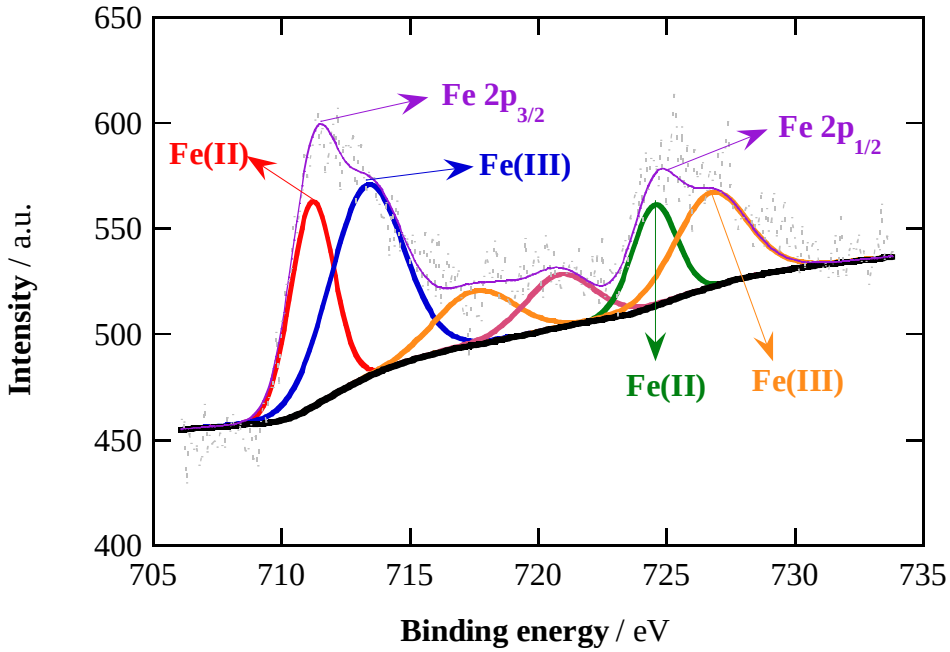
650
600
550
500
450
400
705
710
715
720
725
730
735
Intensity / a.u.
Binding energy / eV
Fe 2p3/2
Fe 2p1/2
Fe(II)
Fe(III)
Fe(II)
Fe(III)

Fig. 7

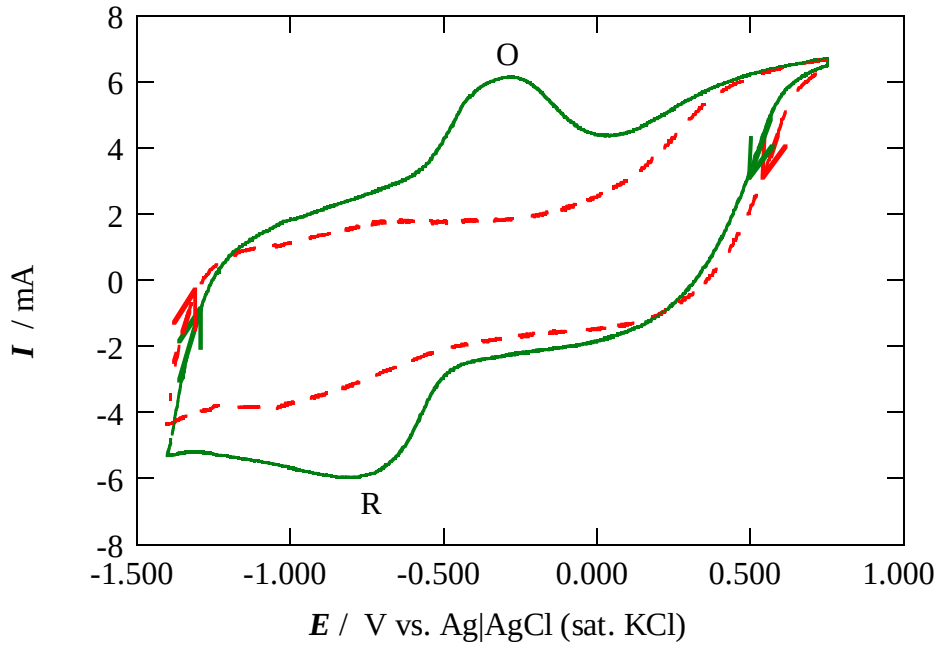
8
6
4
2
0
-2
-4
-6
-8
O
R
-1.500
-1.000
-0.500
0.000
0.500
1.000
I / mA
E / V vs. Ag|AgCl (sat. KCl)

Fig. 8

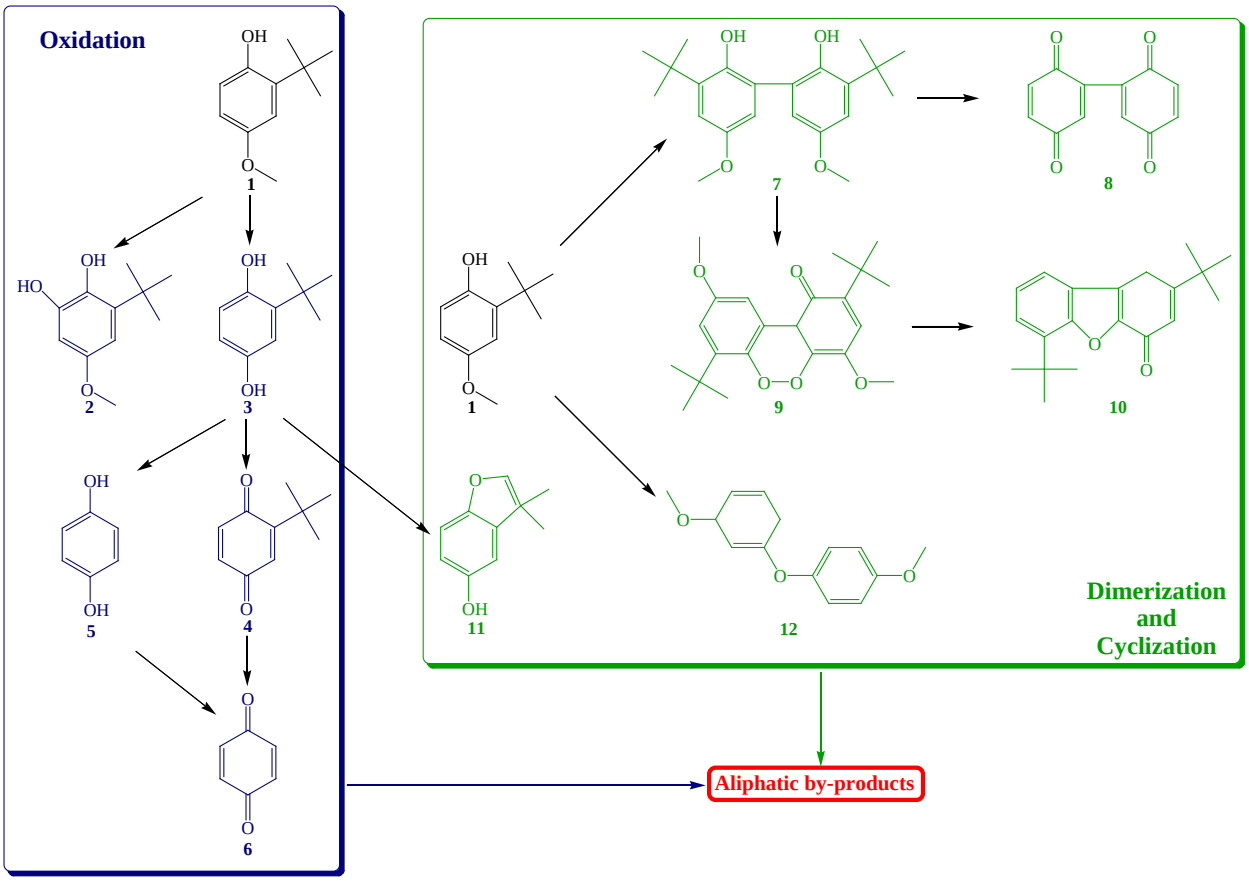
Oxidation
OH
O
1
HO
OH
2
OH
3
OH
5
O
4
O
6
OH
1
OH
OH
7
O
O
8
O
O
9
O
10
O
11
12
Dimerization
and
Cyclization
Aliphatic by-products

Fig. 9

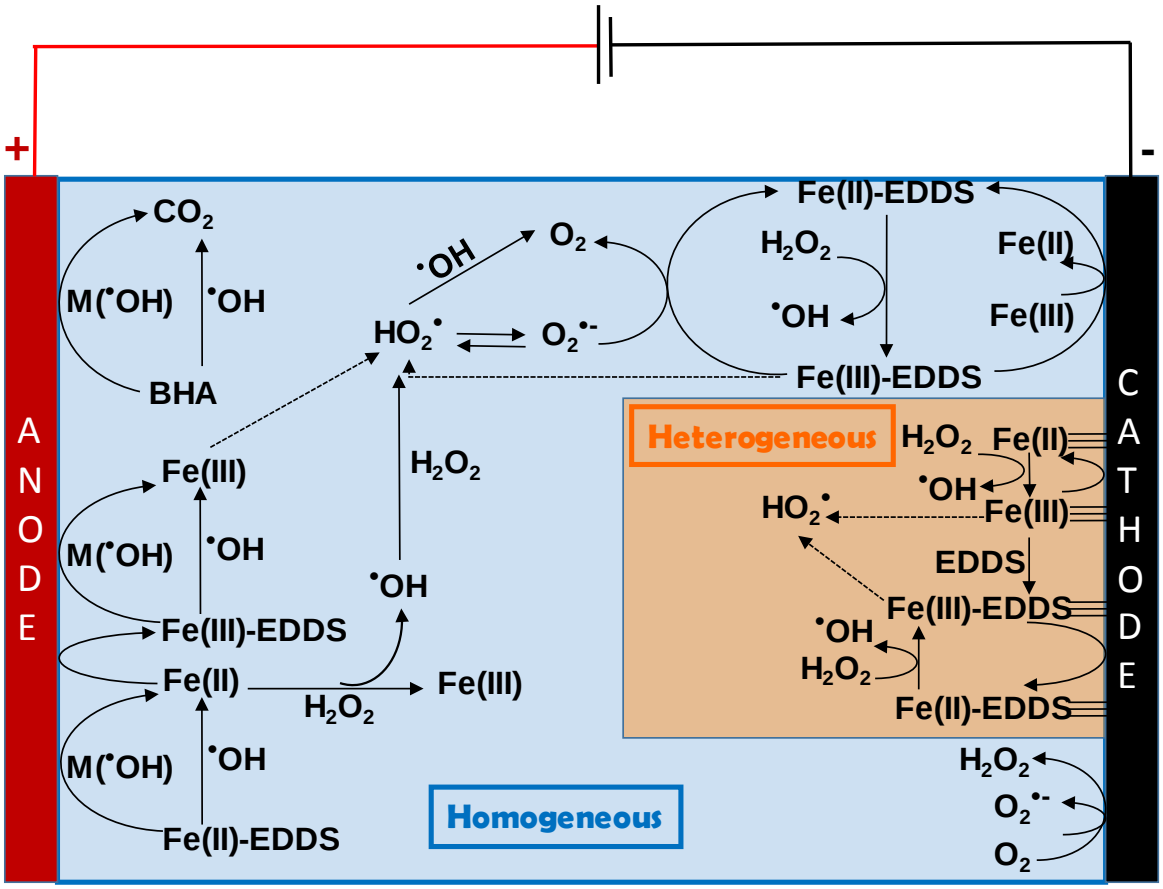
+
-
ANODE
CATHODE
CO2
M(•OH)
•OH
BHA
•OH
O2
HO2•
O2•-
Fe(II)-EDDS
H2O2
Fe(II)
•OH
Fe(III)
Fe(III)-EDDS
Heterogeneous
H2O2
Fe(II)
•OH
HO2•
Fe(III)
EDDS
Fe(III)-EDDS
•OH
H2O2
Fe(II)-EDDS
Fe(III)
M(•OH)
•OH
Fe(III)-EDDS
H2O2
•OH
Fe(II)
H2O2
Fe(III)
M(•OH)
•OH
Fe(II)-EDDS
Homogeneous
H2O2
O2•-
O2

Fig. 10